Metrol. Meas. Syst., Vol. XXII (2015), No. 4, pp. 601–619.

PAN POLSKA AKADEMIA NAUK

METROLOGY AND MEASUREMENT SYSTEMS

Index 330930, ISSN 0860-8229

www.metrology.pg.gda.pl

M&MS

A HIGH PERFORMANCE DIGITAL TIME INTERVAL SPECTROMETER: AN EMBEDDED, FPGA-BASED SYSTEM WITH REDUCED DEAD TIME BEHAVIOUR

Mohammad Arkani

Nuclear Science & Technology Research Institute (NSRTI), Tehran, Iran (✉ markani@aeoi.org.ir, + 98 21 82 061)

Abstract

In this work, a fast 32-bit one-million-channel time interval spectrometer is proposed based on *field programmable gate arrays* (FPGAs). The time resolution is adjustable down to 3.33 ns (= T, the digitization/discretization period) based on a prototype system hardware. The system is capable to collect billions of time interval data arranged in one million timing channels. This huge number of channels makes it an ideal measuring tool for very short to very long time intervals of nuclear particle detection systems. The data are stored and updated in a built-in SRAM memory during the measuring process, and then transferred to the computer. Two *time-to-digital converters* (TDCs) working in parallel are implemented in the design to immune the system against loss of the first short time interval events (namely below 10 ns considering the tests performed on the prototype hardware platform of the system). Additionally, the theory of multiple count loss effect is investigated analytically. Using the Monte Carlo method, losses of counts up to 100 *million events per second* (Meps) are calculated and the effective system dead time is estimated by curve fitting of a non-extendable dead time model to the results (τ_{NE} = 2.26 ns). An important dead time effect on a measured random process is the distortion on the time spectrum; using the Monte Carlo method this effect is also studied. The uncertainty of the system is analysed experimentally. The standard deviation of the system is estimated as ± 36.6 × T (T = 3.33 ns) for a one-second time interval test signal (300 million T in the time interval).

Keywords: time interval spectrum, stochastic process, TDC, dead time effect, Monte Carlo simulation, FPGA.

1. Introduction

Different analyses have been performed on the signals formed by nuclear radiation detection systems, such as analysis of the pulse height spectrum, a time coincidence of the detected particles, the time interval spectrum of the reactions, accumulated counts in a time interval, *etc*. The major rule of nuclear events is their stochastic nature, which usually obeys the Poisson statistics. Taking the nuclear decay process as an example, it is a fundamentally binary random process which is adequately described by the Poisson distribution (if the observation time is adequately short in comparison with the half-life of radionuclide) [1]. The essential properties of a physical process obeying the Poisson statistics are independence and stationariness. Nevertheless, the process is not stationary when $\lambda t \gtrsim 1$ (λ: the decay constant of a radionuclide, t: time) [2]. In multiplying media, the statistics deviates from the Poisson distribution due to the chain correlative neutrons, while background counts have a constant distribution over the time intervals between pulses [3]. The processes considered in the present work are assumed to be the stationary Poisson processes with zero correlation in time.

There is a variety of different applications assigned to the time interval spectrometers in nuclear experiments, a few of them are mentioned below:

– System adjustment and its features (like physical characteristics) may cause a distortion of the statistical properties of an experimental time interval spectrum. The distortion cannot be

- 10.1515/mms-2015-0048

Article history: received on Jun. 30, 2015; accepted on Sep. 16, 2015; available online on Dec. 07, 2015; DOI: 10.1515/mms-2015-0048.

recognized by the pulse height spectrum or by the integral counting data of the detector as the problem is folded in the timing features of the results.

– After-pulses might be a result of a bad adjustment of the system parameters. They are another type of noise sometimes observed in pulse mode radiation detection systems. After-pulses are spurious pulses that appear in the wake of true pulses, *e.g*. a pulse of electrons in a photomultiplier sometimes generates succeeding spurious pulses, called after-pulses. These are detrimental to statistical analysis of the distribution of the particle counts. One or more after-pulses may follow every true pulse. The after-pulse amplitude does not vary with respect to the incident radiation energy. Examination on after-pulsing is only possible by appliaction of time interval spectrometers.
– Research on high-order effects of the system dead time in the processing of nuclear detector signals is a vitally important application of time interval spectrometers [4, 5].
– The dead time can be estimated by the *time interval distribution* (TID) method [6]. As the dead time distortion is highly limited to the short time intervals, a curve fitting to the data in the lengthy time interval region returns a very good estimation of the original process. The method is accurate and applicable for all kinds of radiation detectors with no potential difficulty and no need for any specific nuclear facility. This is not a time-consuming method and offers an advanced capability of online examination during normal operation of the detection system.

Every detection and measuring instrument working in the pulse mode shows an individual time constant taking a specific time for recovery. The counter is insensitive to the following pulses until a period equal to or greater than the resolving time has elapsed. This is the definition of the system dead time, which not only causes the loss of counts but also results in distortion on the experimental distribution of the time intervals. Since the dead time effect is vitally important in experimental stochastic physics, a considerable amount of effort has been taken to understand the effects of dead time and its correction employed such tools as the operational calculus and renewal theory [7, 8]. The error originated from the dead time is a systematic error in counting measurements. Correction of dead time losses must be taken into account when the loss rate is significant. Estimation of true counting rates with a quantitative and qualitative analysis is a particular aim accomplished with the use of appropriate dead time models. The losses of counts are mainly due to the pile-up reject time, the extendable or non-extendable system dead time or a complex combination of these well-known phenomena. The extendable and non-extendable models are widely used for correction of counting rate losses considering the dead time behaviour of the detection system [9]. Recently, some especial efforts are aimed at improving the efficiency of these models which are validated experimentally [10, 11]. Furthermore, a method based on artificial neural networks is successfully tested in experiment [12].

Traditional nuclear instrumentation modules are matured and are standardized lately. A general attitude towards modernization and refurbishment of the instruments using digital technology is gaining momentum since complex programmable silicon devices are introduced. As the best solution for problems related to the nanosecond timing experiments is implementing logic circuits in programmable hardware, applications of *field programmable gate arrays* (FPGAs) are spreading. In this work, a prototype time interval spectrometer is designed based on this technology. The design is capable of collecting data in one million data channels, making it a sophisticated tool for very short time to very long time intervals. As two parallel *time-to-digital converters* (TDCs) are employed for time-to-digital conversion, the dead time of the system is effectively tolerated. The problem is investigated analytically and a formula for the observation probability of multiple short time intervals during T_n (the non-extendable dead time of each TDC) is derived. The behaviour of the parallel TDCs (the count losses and the distortion of the resulting time interval spectrum) is simulated by the Monte Carlo method and the response of

the system is anticipated at different event rates of the measuring random process. Finally, the uncertainty of the system is evaluated experimentally in an appropriate way.

In Section 2, a brief description of the principle of time interval spectrometers is given. The description helps readers to have a better understanding of the design and its comparison with the previous technology. The system structure is explained in Section 3. In Section 4, the observation probabilities of multiple counts during the system dead time is investigated analytically. Additionally, the count losses and distortion of the measured spectrum due to the system dead time are simulated using the Monte Carlo method. The uncertainty of the system is studied experimentally in Section 5. Finally, Section 6 contains the conclusions.

2. Principles of time interval measurement

2.1. Time-to-amplitude conversion

The traditional method of time interval spectrum measurement in nuclear electronics is based on application of *time-to-amplitude converter* (TAC) units. Using TAC units, the time is converted to the pulse amplitude proportionally. Fig. 1 shows the general principle of time-to-amplitude conversion used in nuclear TAC units [13]. The converter capacitor is charged by a constant DC current source after the start signal is triggered (the normally closed start switch is opened by triggering). The buffer prevents the loading effect on the voltage of the capacitor. Therefore, the output voltage of the first stage increases linearly in a ramp shape during the time interval. When the stop signal is triggered, the charging process is stopped. The voltage transient during the time is shown on the figure at the output of the first stage of the circuit.

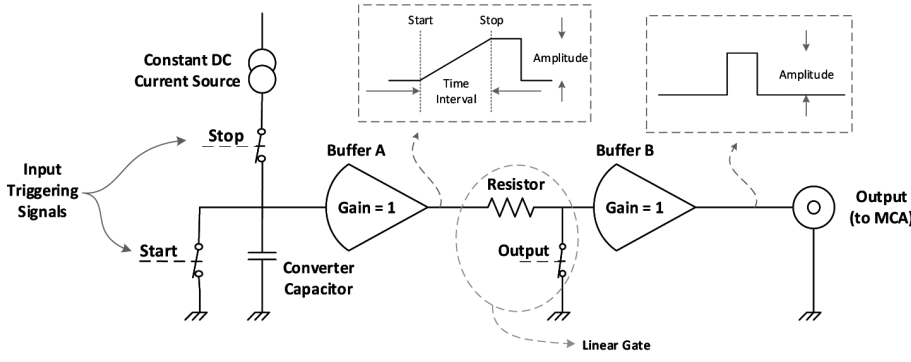

Fig. 1. A general schematic of time-to-amplitude conversion.

Figure 2 shows the experimental set-up for measurement of the time interval spectrum. Events are detected by the pulse mode radiation detector and the signal is amplified and discriminated by the preamplifier/amplifier and the time pick-off modules, respectively. The preamplifier accepts the single detector output and delivers isolated outputs for timing and pulse height or practicle energy measurements. This scheme preserves the low noise required for pulse-height spectroscopy, while offering a fast rise time for time spectrometry. The nuclear random process is provided at the output of the time pick-off module in the form of logic pulses. For a single output detector (no start and stop signals), the system demonstrated in Fig. 2 provides a practical solution. Using a TAC unit, the time intervals are converted into the proportional pulse amplitudes. A *multichannel analyser* (MCA) measures the pulse height spectrum. As this is a proportional method, x-axis must be calibrated in time intervals, *e.g.* using a known deterministic or stochastic process.

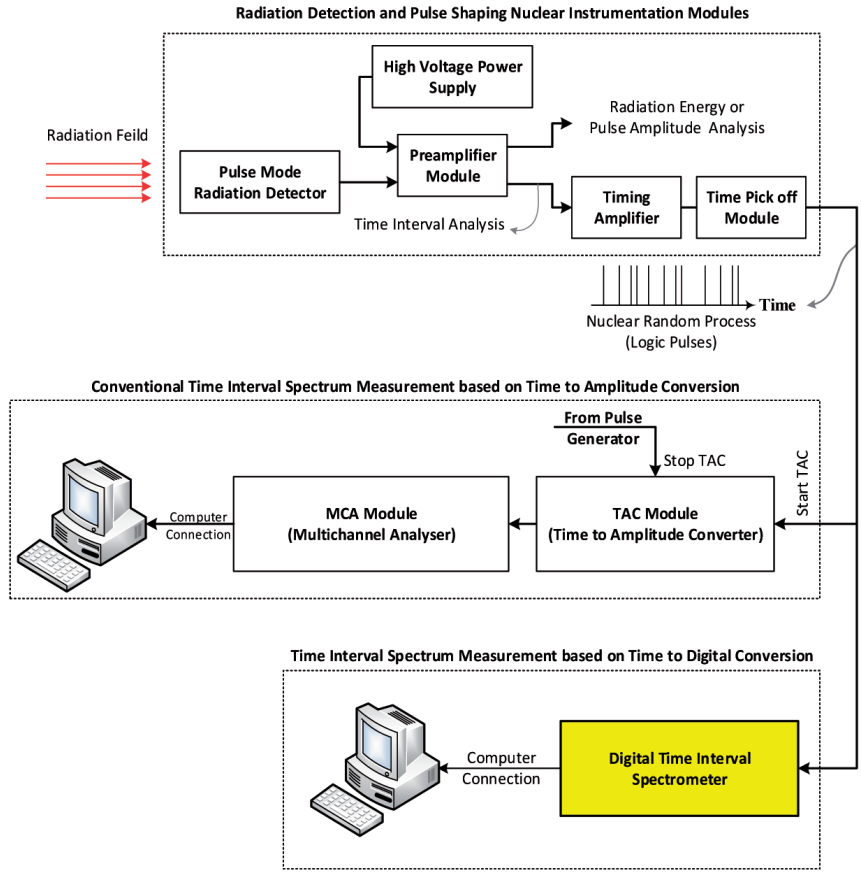

Fig. 2. A general set-up for the time interval spectrum measurement based on standard nuclear electronic modules and a digital time interval spectrometer.

A linear gate composed of a resistor and a normally closed switch is opened after the time interval has elapsed. Therefore, a pulse with its amplitude proportional to the time interval appears at the output of the second stage. The waveforms are shown in the figure. In this method, the shape of the pulse height spectrum is equivalent to the shape of the time interval spectrum of the pulses.

2.2. Conversion of time intervals into digital quantities

The principle of TDCs is explained in the published literature covering a range of different applications [14–23]. In this work, time intervals between consecutive pulses are converted into digital quantities. Therefore, each leading edge of the arriving pulses ends the previous conversion and starts the next conversion process. During these transactions, the system might not be responsible for the next detected events; this period is defined as the system dead time. To moderate the dead time effect of the system, the conversion is performed by two identical individual TDC hardware modules. Each module is involved in a conversion process solely while the other one is in the standby mode. For the next time interval conversion, the role of the modules is swapped. During the progress of conversion, the measured data from the previous conversion is captured and is processed to update the time interval spectrum data.

Figure 3 shows the method employed in this work. The random process is synchronized with the system clock. Then the time intervals are processed by the TDCs in turn. After that, the data are fetched and processed by the final stage to form the spectrum of data and to communicate with the computer. More details about the system architecture will be given in the following sections. In Fig. 4, three events are detected and recorded by the system. This figure shows functioning of the two TDCs. The non-extendable dead time, T_n, refers to the duration that each TDC is involved in interfacing with its following modules, transmission of measured data and reset process. Whenever one of TDCs is unresponsive to the next event, the other one is ready to record the second short time interval event. The third (and the other preceding consecutive short time intervals) consecutive short time interval event is lost and cannot be recorded by this architecture. More details about loss of events by the system are explained in Section 4.

In Fig. 2, the experimental set-up for a digital time interval spectrometer is shown. Unlike the time-to-amplitudeconversion method, which also needs a MCA module for data acquisition and time calibration, using a TDC-based equipment for measuring the time interval spectrum, makes the experiment simpler and no timing calibration is needed. Usually, a precise quartz crystal oscillator is employed by TDCs to discretise the time. General information about the conversion error and its uncertainties in TDCs is published elsewhere [24–26]. The uncertainty of the system is examined experimentally and the results are reported in Section 5.

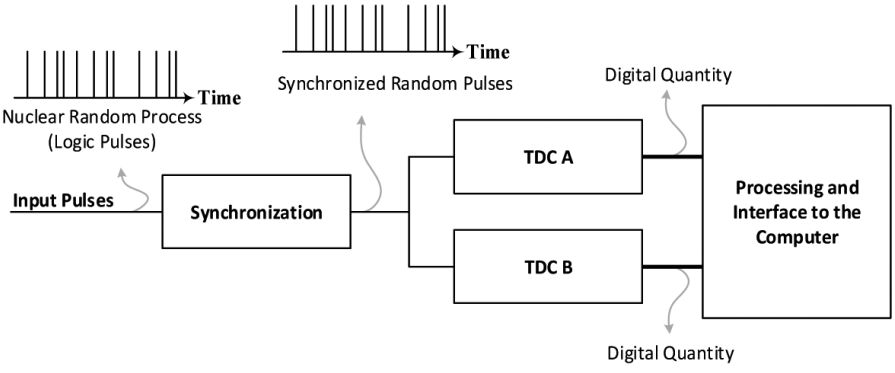

Fig. 3. The general schematic diagram of the innovative digital time interval spectrometer implemented in this work.

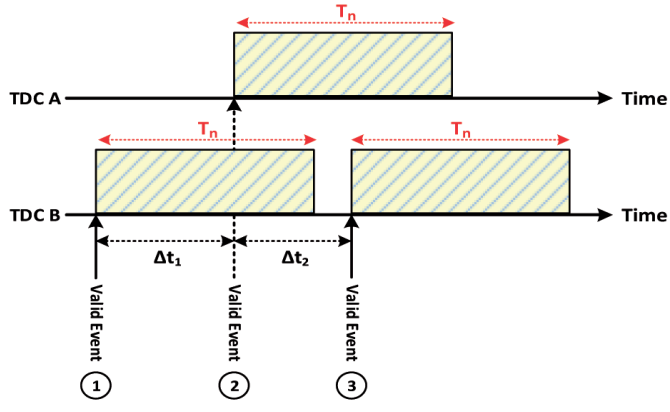

Fig. 4. The timing transient of the two TDCs for three consecutive random events. Three valid events are recorded by the system.

3. System structure

A simplified structure of the system is shown in Fig. 5.

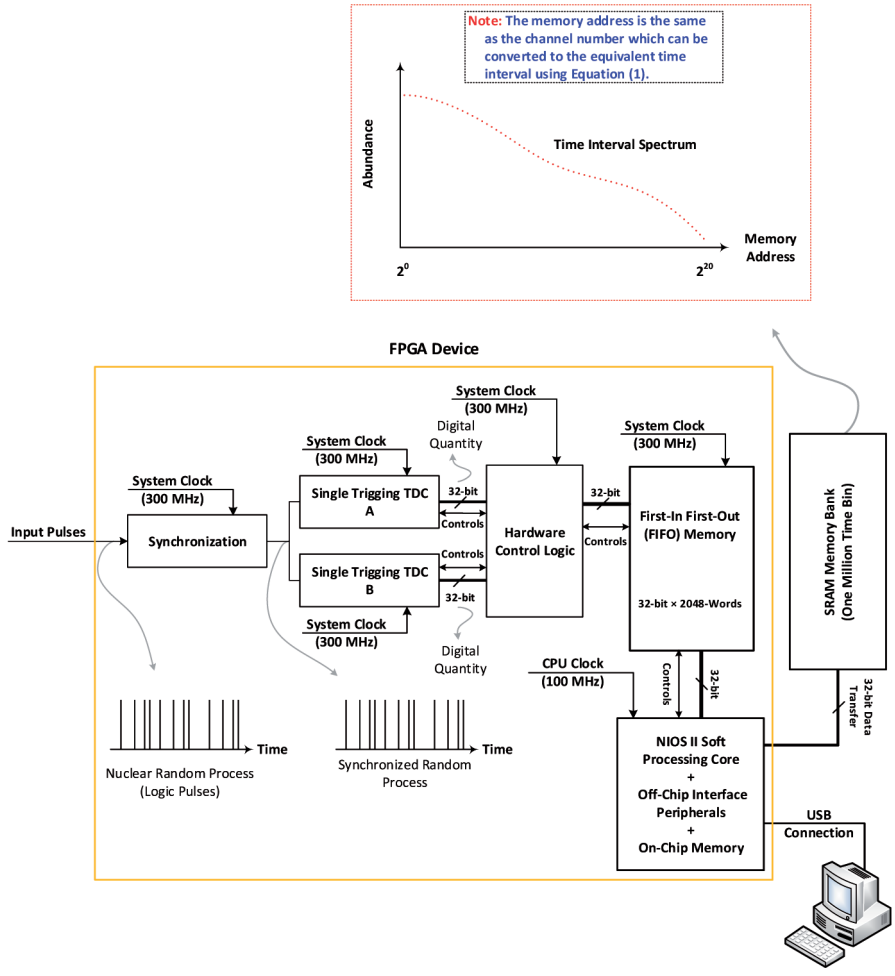

Fig. 5. A simplified structure of the system.

The heart of this system is the FPGA device, which is a CYCLONE III family device (CYCLONE III is one of the families of the FPGA products of ALTERA Corporation. The part number of the device is EP3C25Q240C8N) [27]. Each time one of the two TDCs converts the time interval to a digital quantity. During the conversion, the data measured by the other TDC are fetched and written into the FIFO memory by the hardware control logic block. This ensures a zero dead time of the measuring equipment for the first short time interval events. The data written in the memory are read and processed by the NIOS II soft processing core [28, 29]. The system provides one million channels for accumulation of the spectrum data. The data from each channel are stored at one of the addresses of the memory. Each time interval falls in one of the timing channels. Therefore, the processor increments the data stored at the corresponding address. The time resolution or channel width is determined by the clock of the TDCs, which is limited by the speed features of the device. For the case of the FPGA component used in the

presented work, the maximum digitization frequency is 300 MHz (corresponding to the time resolution of 3.33 ns). A general formula can be written for the relation between the maximum acquirable time interval and the channel width of the system as:

$$T_{\max} = N_{Ch} \times \Delta T_{Ch} = 2^{20} \times \Delta T_{Ch}, \tag{1}$$

where: T_{max} is the maximum measurable time interval; N_{Ch} is the number of channels of the equipment (in this work, $N_{Ch}=2^{20}$); and ΔT_{Ch} is the channel time width. Note, that N_{Ch} depends on the capacity of dedicated SRAM memory. Therefore, one million channels means the space for storage of one million 32-bit data. For ΔT_{Ch} equal to 3.33 ns, the maximum acquirable time interval is around 3.49 ms. As it takes three digitization periods to complete each sampling process, the maximum dead time of each TDC is $3\times T$ $\left(T_n = 3\times 3.33\ ns = 10\ ns\right)$.

4. Effects of system dead time

In nuclear random processes, the time interval between consecutive events is down to zero, *e.g.* decaying of a radioactive gamma source, which obeys the Poisson statistics. According to the system architecture, if several consecutive short time interval events occur, only the first two short time interval events are recorded. The term of short time interval refers to the time intervals less than T_n (< 10 ns). An example of such a condition is shown in Fig. 6.

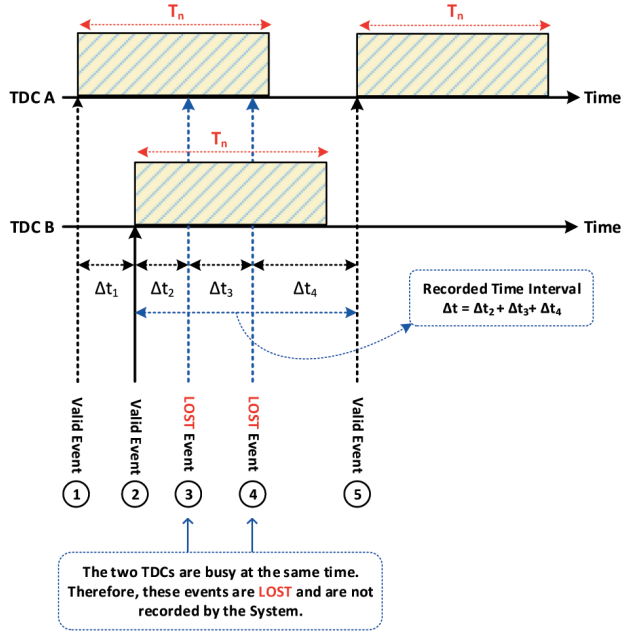

Fig. 6. Loss of events due to the system dead time. The architecture can preserve the first two short time interval events, but the next short time intervals are missed.

The first and the second short time interval pulses are recorded, but the third and the fourth ones are lost due to the non-extendable dead time behaviour of the TDC modules. For the fifth one, the TDC A is ready and it is recorded. Therefore, instead of recording three short time intervals, a longer time interval is registered $\left(\Delta t = \Delta t_1 + \Delta t_2 + \Delta t_3\right)$ which leads to some side effects on the resulting experimental spectrum as:

– Some of the short time interval events are not recorded (refer to Fig. 6, the third and the fourth consecutive short time intervals); therefore, they are missed in the measured spectrum.
– Instead of the missed short time interval events, a longer time interval is recorded, which causes a shift in the time interval spectrum. Usually, the random process is uncorrelated; therefore, the shifted spectrum has a constant probability for all time intervals throughout the spectrum. More details about the distorted Poisson process is published elsewhere [6].

Missing some of short time interval events changes the resulting distribution into a new type of distribution. For instance, in a Poisson random process, the variance to mean ratio of the counts is equal to unity. Nonetheless, measuring the process by a measurement system with a specific dead time causes a deviation from the Poisson process. This is the subject of some research works on estimation of the dead time of nuclear radiation systems [30, 31].

As two parallel TDCs are employed, the dead time problem represented in this work is a special case. Therefore, no analytical formulation is given for the problem in the literature. In Section 4.1, the observation probabilities of multiple counts are studied analytically and a general formula is derived. Losses of counts and distortion of the spectrum are also investigated numerically using the Monte Carlo method; the detailed description of the results is given in Section 4.2.

4.1. Multiple consecutive short time intervals and theoretical analysis

Multiple events during the system dead time are possible, since there is a higher probability of occurring short time interval events in nuclear random processes. In most cases, the Poisson *probability distribution function* (PDF) is a random process in nuclear applications. The Poisson PDF for time intervals between events is defined as [9]:

$$f\left(n,T_n\right)=n\ e^{-n\,t}, \tag{2}$$

where: $f\left(n,T_n\right)$ is the Poisson PDF for time intervals, n is the true counting rate, and t is the time parameter. The overall observation probability of occurring random events during T_n, is easily calculated by integration of (2) over the time domain as:

$$P\left(n,T_n\right)=1-\ e^{-n\,T_n}. \tag{3}$$

The probability of time intervals greater than T_n is then calculated as:

$$1-P\left(n,T_n\right)=e^{-n\,T_n}. \tag{4}$$

Now, suppose that P_m is the observation probability of m consecutive events during T_n. Then, the summation over all cases of P_m is equal to $P(n, T_n)$:

$$P\left(n,T_n\right)=\sum_{m=1}^{\infty}P_m\left(n,T_n\right). \tag{5}$$

In order to obtain a general analytical formula for P_m, the problem is solved for the first three cases of m (m = 1, 2, 3) as follows. Then, by induction, the general formula is derived.

Case I (m = 1): Consider the process shown in Fig. 7. Although the time interval between the first and second events is shorter than T_n, they are both the valid events owing to the system architecture. Note, that P_{inf} is the observation probability of the first event after T_n (the last multiplying term in (6), (8), and (10)). This is simply described by (6), the relation which gives the observation probability of a single event within dt':

$$P_1(t',n,T_n)\,dt' = \left(e^{-n\,t}\right) \times \left(ndt'\right) \times \left(e^{-n(T_n-t')}\right). \tag{6}$$

Note, that the definitions for t' and dt' are shown in Fig. 7 graphically. $P_1(t',n,T_n)$ is the probability of observation of a single event at the moment t' within the period T_n. Integration of this equation over the time domain gives $P_1(n,T_n)$, the probability of observation of a single event during T_n. The result is expressed by (7).

$$P_1(n,T_n) = \int_0^{T_n} e^{-n\,t'} n e^{-n(T_n-t')} dt' = nT_n e^{-nT_n}. \tag{7}$$

Case II (m = 2): Fig. 8 shows the process in which three consecutive short time interval events are observed during T_n. Similar to (6), the probability distribution function for $P_2(t',t'',n,T_n)$ can be written as:

$$P_2(t',t'',n,T_n)\,dt'\,dt'' = \left(e^{-n\,t'}\right) \times \left(ndt'\right) \times \left(e^{-n\,t''}\right) \times \left(ndt''\right) \times \left(e^{-n(T_n-t'')}\right). \tag{8}$$

$P_2(t',t'',n,T_n)$ is the probability of observation of two consecutive events at t' and t''. By integration over the time domain, the probability of observation of two consecutive events during T_n is obtained as:

$$P_2(n,T_n) = \int_0^{T_n}\int_{t'}^{T_n} n^2\, e^{-n\,t'}\, e^{-n\,t''}\, e^{-n(T_n-t'')}\, dt'\, dt'' = \frac{n^2\, T_n^2\, e^{-nT_n}}{2}. \tag{9}$$

Case III (m = 3): Similar to the previous cases, according to Fig. 9, $P_3(t',t'',t''',n,T_n)$, the probability of observation of three consecutive events at t', t'', and t''' during T_n can be expressed as:

$$\begin{aligned} &P_3(t',t'',t''',n,T_n)\,dt'\,dt''\,dt''' = \\ &\left(e^{-n\,t'}\right) \times \left(ndt'\right) \times \left(e^{-n\,t''}\right) \times \left(ndt''\right) \times \left(e^{-n(t''')}\right) \times \left(ndt'''\right) \times \left(e^{-n(T_n-t''')}\right) \end{aligned} \tag{10}$$

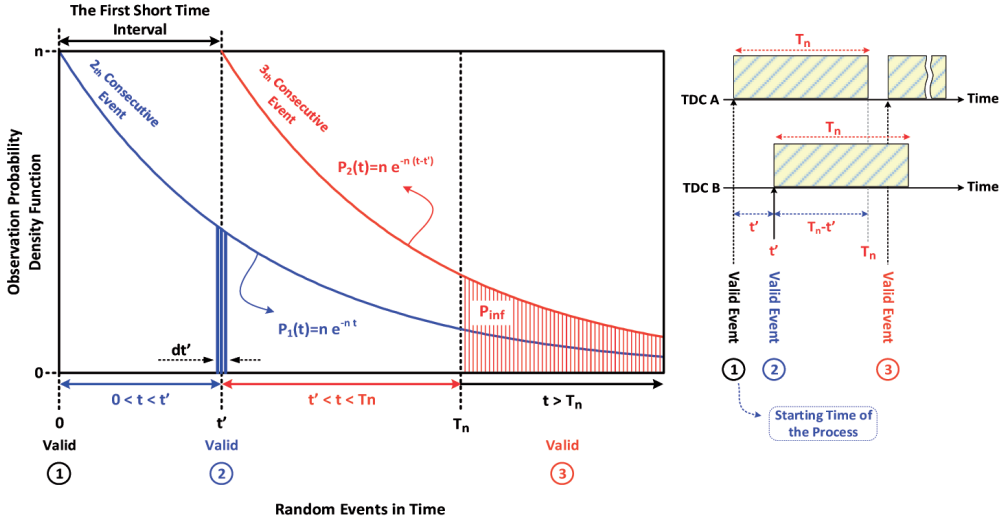

Fig. 7. Two consecutive Poisson random events during T_n, the first event is recorded by TDC A and the second one by TDC B, no event is lost by the system.

- 10.1515/mms-2015-0048

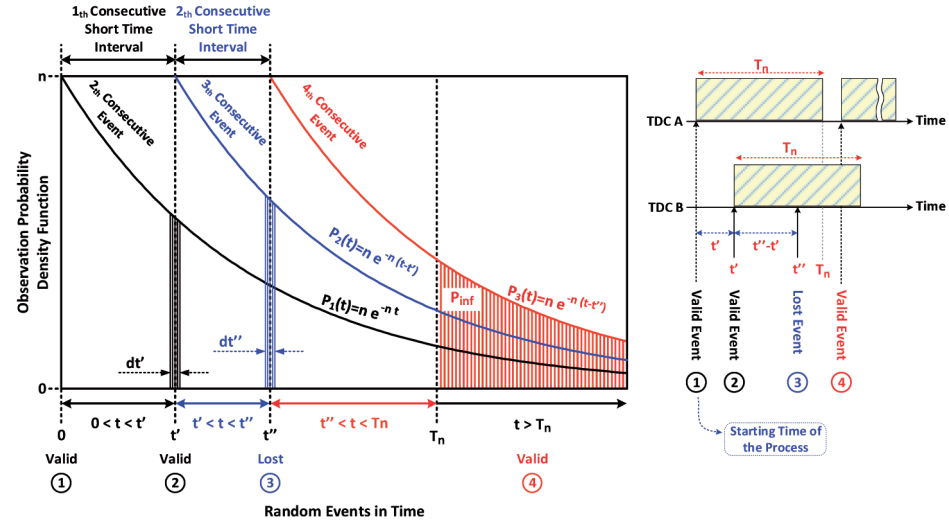

Fig. 8. Three consecutive Poisson random events during T_n, the first two events are recorded by the system, but the third one is lost. The last one is recorded by TDC A as it occurs at $t > T_n$.

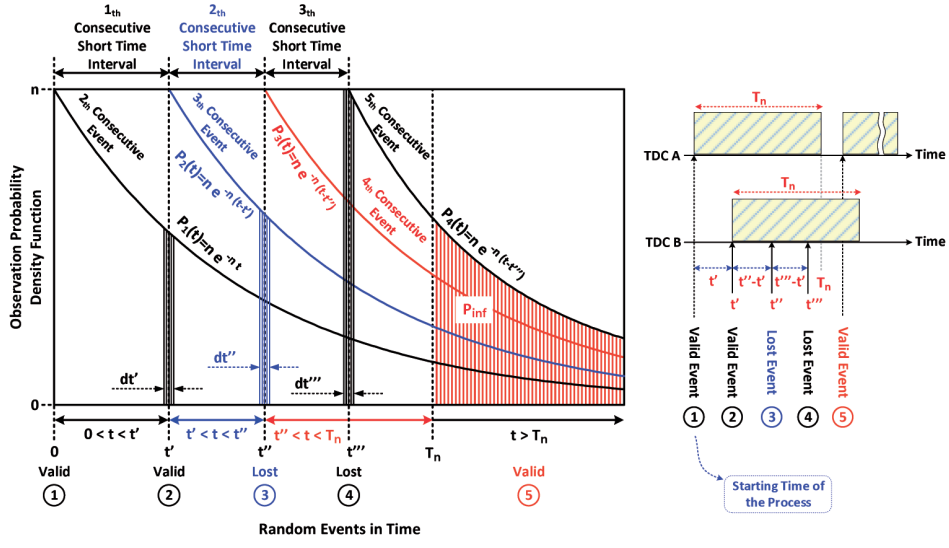

Fig. 9. Four consecutive Poisson random events during T_n. The third and fourth events are lost.

The definitions of other parameters of (10) are expressed in Fig. 9 graphically. Integration of (10) over the time domain results in (11), the probability of observation of three consecutive pulses during T_n is:

$$P_3(n,T_n) = \int_0^{T_n}\int_{t'}^{T_n}\int_{t''}^{T_n} n^3\, e^{-n\,t'}\, e^{-n\,t''}\, e^{-n\,t'''}\, e^{-n(T_n-t''')}\, dt'\, dt''\, dt''' = \frac{n^3\, T_n^3\, e^{-nT_n}}{6}. \qquad (11)$$

General Formula: Using the results obtained from the above cases, the general formula can be derived by mathematical induction as:

$$P_m\left(n,T_n\right) = \frac{n^m\ T_n^m\ e^{-nT_n}}{m!}. \tag{12}$$

The definitions of parameters are the same as in the previous equations. Summation over the infinite number of m gives:

$$P\left(n,T_n\right) = e^{-nT_n}\sum_{m=1}^{\infty}\frac{n^m\ T_n^m}{m!}. \tag{13}$$

Using the Taylor expansion for e^{nT_n}, (14) is obtained:

$$\left(1+nT_n+\frac{n^2T_n^2}{2}+...+\frac{n^kT_n^k}{k!}+...\right)=e^{nT_n},\ k=\text{zero, 1, 2, ...} \tag{14}$$

Inserting of (14) into (13), with a little mathematical simplification, results in:

$$P\left(n,T_n\right) = e^{-nT_n}\sum_{m=0}^{\infty}\frac{n^m\ T_n^m}{\text{m!}}-e^{-nT_n}=e^{-nT_n}\left(1+nT_n+\frac{\left(nT_n\right)^2}{2}+...+\frac{\left(nT_n\right)^k}{k!}+...\right)-e^{-nT_n} \tag{15}$$

$$=e^{-nT_n}e^{nT_n}-e^{-nT_n}=1-e^{-nT_n}.$$

The result is the same as (3), the probability of observation of any event during T_n. Considering the structure of the equipment developed in the presented work, after the first short time interval events have been recorded the observation probability of occurring the pulses during T_n is changed into (16):

$$P_s\left(n,T_n\right) = e^{-nT_n}\sum_{m=2}^{\infty}\frac{n^m\ T_n^m}{m!}=1-e^{-nT_n}-nT_ne^{-nT_n}. \tag{16}$$

In the worst case, T_n = 10 ns, n = 100 Meps, the observation probability is around 63.2 percent for all time intervals shorter than T_n, if only a single TDC is implemented in the structure (all short time interval events during T_n). This is reduced to the value of 0.2642 if two TDCs are implemented (all short time interval events during T_n except for the first one). For the case with the third parallel TDC added, this probability value is 0.083 (all short time interval events during T_n except for the first two short time interval events). For the two extremal cases (n = 1 and n = 100 Meps), $P_m(n,\ T_n)$ is calculated and shown in Fig. 10 graphically. In this figure, the parameter m versus the observation probability is plotted. In Fig. 11, the observation probabilities of m consecutive pulses during T_n ((12)) against different values of $n \times T_n$ are plotted. In addition, the overall probabilities ((13) and (16)) are plotted and compared with each other.

4.2. Monte Carlo simulation of dead time effect

Monte Carlo is a powerful statistical method. The basic theory of the method and its applications for dead time problems are given in a variety of scientific works [6, 32–35].

In stochastic experiments, the properties of input stochastic process are unknown. Therefore, the distorted Poisson process measured by the equipment cannot be compared with the original one. In radiation studies in which the information about the original stochastic process is of a vital importance, the Monte Carlo method is an advantageous solution allowing precise comparison of the results. This is an important feature of the method, especially for simulation of the dead time effect [6, 32].

The algorithm shown graphically in Fig. 6, based on the Monte Carlo method, is translated to the MATLAB [36] m-code. The pseudorandom number generator is rand() function in MATLAB software. Two important side effects of the system dead time are simulated, the event loss rate and the dead time distortion of the time interval spectrum. The results are given in the following subsections.

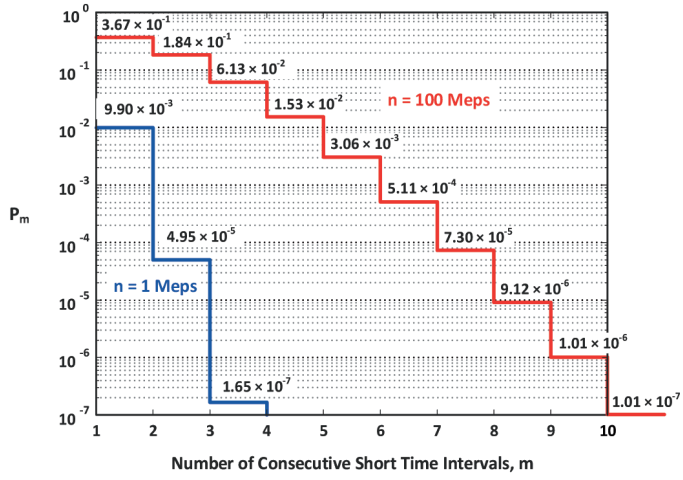

Fig. 10. The observation probabilities (P_m) of a different number of multiple short time interval events at two different true event rates, based on (12). Note, that the first two short time interval events (m = 0, 1) are recorded by the parallel TDCs.

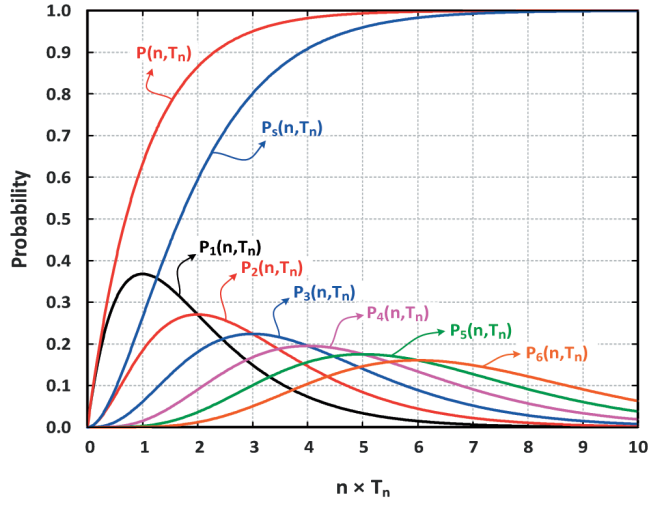

Fig. 11. The observation probabilities of m consecutive pulses during T_n ((12)) against different values of $n \times T_n$. The overall probabilities ((13) and (16)) are plotted and compared with each other.

4.2.1. Losses of events due to system dead time

In order to study the dead time losses, from 100 keps up to 100 Meps, at 101 different event rates, each event rate being a multiple of one million Poissonian time intervals, the problem has been simulated. The results are shown in Fig. 12. For the first few Meps of the random

event rates, the loss rate is negligible. Therefore, the true event rate and the response of the parallel TDCs are nearly the same. At 100 Meps, count losses of the system are equal to around 20 Meps which means that 80 Meps is the observed event rate using two parallel TDCs. The non-extendable dead time model is fitted to the curve and the equivalent dead time parameter is estimated to be 2.26 ns. Fig. 12 shows the response of a single TDC (T_n = 10 ns) as well. At 100 Meps, application of a single TDC results in a big loss in the observed event rate (around 50 Meps). For a better demonstration, the ratios of a single TDC response and two parallel TDCs response to the true event rate are shown in Fig. 13. At the worst conditions (at the event rate equal to 100 Meps), the deviation from the true event rate for the two parallel TDCs is about twenty percent, whereas for a single TDC reaches about fifty percent. The results show that application of two parallel TDCs gives a thirty percent improvement in comparison with a single TDC response (the dashed line in Fig. 13, at the true event rate equal to 100 Meps).

4.2.2. Distortion on the spectrum

The side effect of the system dead time on the time interval spectrum causes two important distortions: missing a number of short time interval events with resulting a shift in the spectrum. At 100 Meps, as a very high working event rate of the system, simulation of the resulting spectrum has been carried out. Note, that in usual nuclear measurements, the event rates of detectors are limited to several hundred thousand events per second; however, there are fast counting detectors such as photon counters (avalanche photo diodes) that enable higher event rates. Fig. 14 shows the numerical results for the time interval spectrum of the system in response to the input Poissonian stochastic process (at the event rate of 100 Meps). Obviously, below 10 ns ($<T_n$) the spectrum is distorted. Moreover, a little shift occurs towards longer time intervals over the time range greater than 10 ns ($> T_n$). The single TDC response is also calculated and plotted in the figure. Below 10 ns, no time interval is observed using a single TDC structure. However, the use of two parallel TDCs results in a relatively good response. More details are shown in Fig. 14.

5. Uncertainty analysis of the system

In the presented work, time is converted into a digital quantity based on coarse counting method. The systematic error of the coarse counting method is $\leq \pm T$. Also, there are other error components affecting the system uncertainty, *e.g*. the clock jitter error. In this section, the accumulated uncertainty of the system is investigated. A major source of error in most digital implementations for timing purposes stems from the system clock uncertainty. The system clock uncertainty includes the jitter error and the frequency tolerance. The clock signal is mostly provided by quartz crystal oscillators.

The jitter uncertainty is the timing variations of a set of signal edges from their ideal values. Jitters in clock signals are typically caused by noise or other disturbances in the system. Contributing factors include the thermal noise, power supply variations, loading conditions, the device noise, and interference coupled from nearby circuits. The error in the frequency is easily determined by accurate classic laboratory measurement tools while estimation of the jitter error is more complicated and needs a specialized equipment. The jitter error is a stochastic uncertainty, while the frequency tolerance is a deterministic error. The jitter error not only affects the accuracy of the results from TDCs, but also may cause fatal errors in digital implementations as the system might be fed with incorrect data at the clock edges. The long-term jitter measures the change in a clock from the ideal position, over several consecutive cycles. The actual number of cycles used in the measurement is application dependent.

The long-term jitter is different from the period jitter and the cycle-to-cycle jitter, because it represents the cumulative effect of jitter on a continuous stream of clock cycles over a long time interval. That is why the long-term error refers to the accumulated system uncertainty. To measure the accumulated uncertainty of timing features of the system, a system test bench has been set up. A general configuration and the system set-up are shown in Fig. 15. Two independent and identical quartz crystal oscillators are employed as clock sources. One of them generates the system clock, whereas the other – the test signal. Outside of the system architecture block, there are two phase locked loops (PLLs) dedicated to multiplication of the clock frequency. Therefore, two independent 300 MHz clock signals are generated with the same error and statistical characteristics. Note, that notations ΔT_{ErrorA} and ΔT_{ErrorB} refer to the error components of the 300 MHz system clock and the test clock signals, respectively. Dividing the test clock by 300×10^6 generates the test signal with the unit frequency and with the accumulated jitter error of $300 \times 10^6 \times \Delta T_{ErrorB}$. This low frequency test signal results in a very good estimation of the system uncertainty. As the two clock features are the same, this is reasonable to assume that:

$$\Delta T_{Error} = \Delta T_{ErrorA} = \Delta T_{ErrorB}. \tag{17}$$

ΔT_{Error} refers to the system error. Accordingly, ΔT_{Error} can be written as a function of the experimental results, ΔT_{ErrorE}:

$$\Delta T_{Error} = \frac{\Delta T_{ErrorE}}{\sqrt{2}}. \tag{18}$$

Applying the division factor of the test signal, the following result is obtained:

$$\Delta T_{ErrorN} = \frac{\Delta T_{ErrorE}}{300 \times 10^6 \times \sqrt{2}}. \tag{19}$$

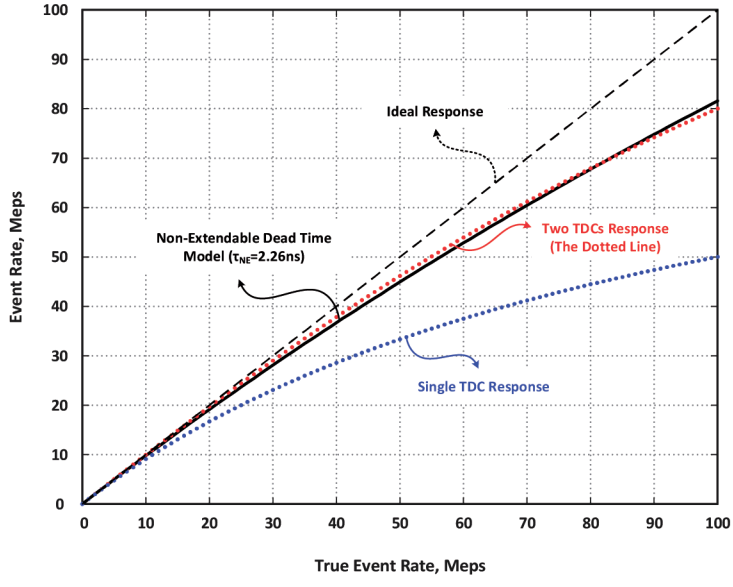

Fig. 12. The observed event rates of the system at different true event rates. The non-extendable model is fitted to the data resulting $\tau_{NE} = 2.26$ ns. Additionally, a single TDC response is plotted for better comparison.

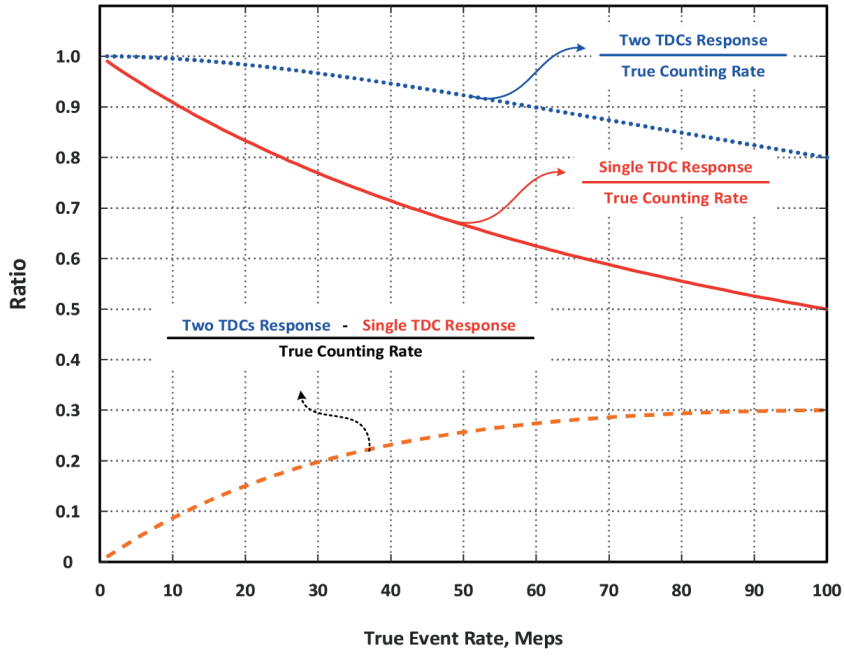

Fig. 13. The ratio of the response of a single TDC and two TDCs to the true event rate.

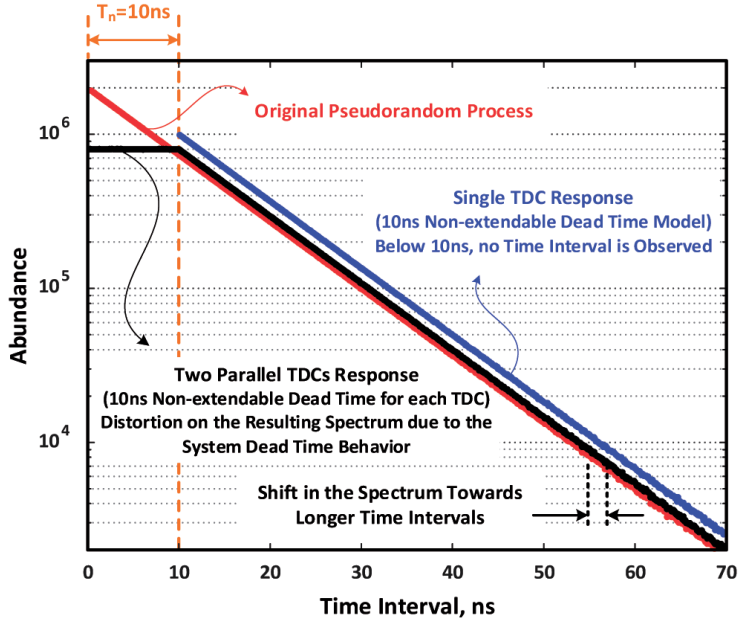

Fig. 14. The spectrum of the time intervals at 100 Meps of the input pseudorandom Poisson process, simulated by the Monte Carlo method. Distortion of the spectrum is limited to the time intervals shorter than 10 ns (the dead time parameter shown in Figs. 4 and 7). Additionally, a little shift on the results is seen (Total number of histories = 200 × 10^6, T_n = 10 ns, n = 100 Meps, Time Bin = 0.1 ns).

- 10.1515/mms-2015-0048

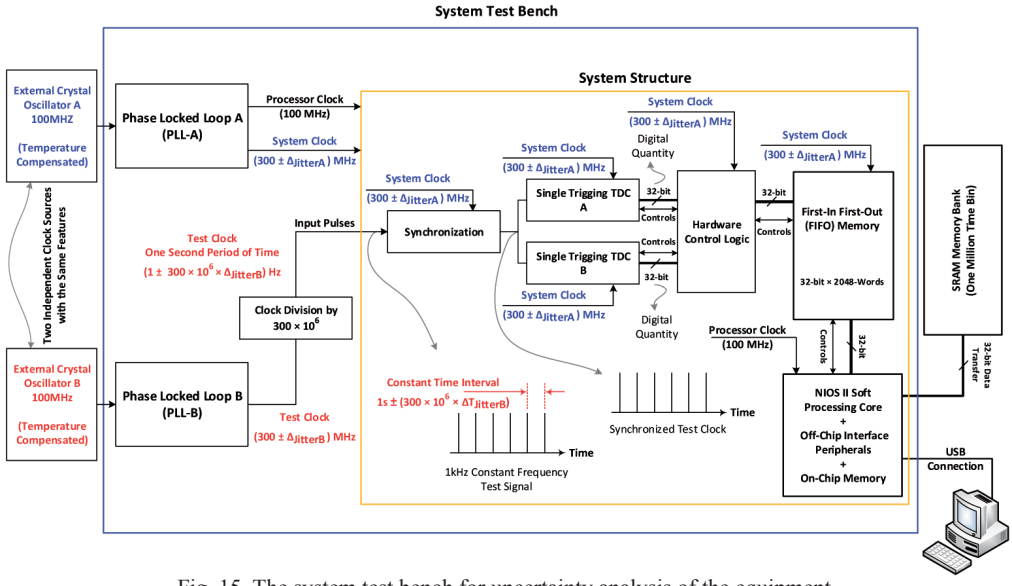

Fig. 15. The system test bench for uncertainty analysis of the equipment.

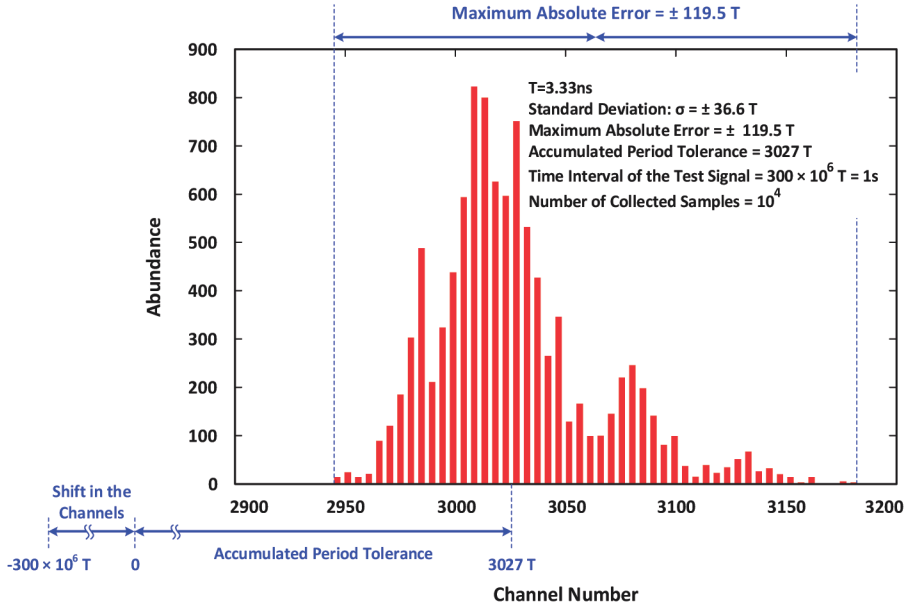

Fig. 16. A histogram of the results for uncertainty analysis of the system.

ΔT_{ErrorN} is the error normalized per T. The system has been tested continuously for ten thousand seconds and ten thousand samples were acquired. Fig. 16 shows the histogram of the data. Note, that the SRAM memory provides one million channels with 3.33 ns time width, which covers 3.49 ms in the whole range. Therefore, one-second time intervals do not fall within the channels. They are shifted numerically before registration in memory. Using the software capabilities of the system, the starting channel is set equal to -300×10^6; this setting is shown in Fig. 16 on the x-axis. Table 1 shows the details of the test results of the system.

Table 1. The system test results for uncertainty analysis (T = 3.33 ns).

Parameter	Experimental Results	
	Values Over One Second Time Interval	Fraction of T (Dimensionless)
Maximum Absolute Error (Refer to Fig. 16)	± 119.5 T [s]	$\pm 3.98 \times 10^{-7}$
Accumulated Standard Deviation, σ	$\Delta T_{Error} = \pm \frac{36.6\ T}{\sqrt{2}} = \pm\ 25.9\ \ T$ [s]	$\Delta T_{ErrorN} = \pm \frac{\Delta T_{Error}}{300 \times 10^6\ T} = \pm 8.63 \times 10^{-8}$
Accumulated Period Tolerance	3027 T [s]	1.01×10^{-5}
Number of Shifted Channels [#]	-300×10^6	
Time Interval of the Test Signal [s]	300×10^6 T (1s)	
Number of Collected Samples [#]	10^4	

6. Conclusion

A very useful instrument in nuclear physics laboratories is a time interval spectrometer, which is traditionally constructed using TACs. Standard nuclear instrumentation modules based on TAC units have been developed lately. There are some advantages and disadvantages of the method, as mentioned below:

– The methodology is old and is not consistent with the state-of-the-art technology.
– For the case of a single detector experiment, an independent pulse generator is also required. Regardless of complications of the hardware and its adjustment, some of the time intervals do not trigger the equipment. Therefore, using TAC units might pose a time-consuming experiment.
– Long-time intervals (no more than a few milliseconds) cannot be measured. The method is best for short time intervals down to the sub-nanosecond range.
– A time-to-digital converter (TDC) unit is connected to the computer directly and does not need any other auxiliary equipment. The time interval measurement based on TAC modules needs a MCA module (and a pulse generator, if a single detector experiment is performed) and – more importantly – time-wise calibration of the system.

In applications in which the sub-nanosecond resolution in time is required, a combined method of time-to-digital conversion is applied. The dead time between consecutive events is an intrinsic feature of discrete-in-time measurement instruments. Since the dead time of nuclear radiation detection systems is in the range of a few nanoseconds to several microseconds, the coarse counting method is employed for time-to-digital conversion in the presented research work.

Owing to the modern technologies of electronic engineering, to answer the needs for high flexibility and high performance applications, digital implementation of the conventional apparatuses is gaining momentum. In this work, a useful, FPGA-based measurement tool is introduced to the scientists. The prototype system resolution for the channel width can be adjusted down to 3.33 ns and provides one-million-channel capacity with minimum total scanning time of 3.49 ms. These features might be adapted in any especial design regarding experimental case studies. To measure very long time intervals, an arbitrary shift in the channels is possible using system capabilities. An important feature is the system dead time.

To tolerate this problem, two parallel TDC modules are implemented in the structure, which perform the conversion process in turn. In Section 4, an analytical formula was derived which describes the observation probabilities of occurring different number of short time intervals during T_n. Additionally, the Monte Carlo simulation was performed to study the distortion of the dead time effect in the observed time interval spectrum. The system dead time is discussed in detail in Section 4. The count loss effect and distortion of the spectrum due to the system dead time are studied using the Monte Carlo method numerically. In Section 5, the uncertainty of the system is investigated experimentally. A test bench was set up using two independent clock sources with the same statistical features. The theoretical formulation of the test is given in the text. The accumulated uncertainty of the system is estimated as $\sigma = \pm 36.6 \times T$ for one-second time intervals ($= 300 \times 10^6\ T$). Similarly, the accumulated period tolerance is estimated as $3027 \times T$. The detailed results of the test are shown in Fig. 16 and Table 1.

References

[1] Evans. R.D., (1962). *The Atomic Nucleus*. McGraw-Hill.

[2] Matthews, I.P., Kouris, K., Jones, M.C., Spyrou, N.M. (1980). Theoretical and experimental investigations on the applicability of the Poisson and Ruark-Devol statistical density functions in the theory of radioactive decay and counting. *Nuclear Instruments and Methods,* 171(2), 369–375.

[3] Thie, J.A. (1963). *Reactor noise*. Rowman and Littlefield, Inc., New York.

[4] Denecke, B., de Jonge, S. (1998). An analyzer for pulse-interval times to study high-order effects in the processing of nuclear detector signals. *Applied Radiation and Isotopes,* 49 (9–11), 1099–1105.

[5] Pomme, S. (1998). Time distortion of a Poisson process and its effect on experimental uncertainty. *Applied Radiation and Isotopes*, 49(9–11), 1213–1218.

[6] Arkani, M., Raisali, G. (2015). Measurement of dead time by time interval distribution method. *Nuclear Instruments and Methods in Physics Research, Section A: Accelerators, Spectrometers, Detectors and Associated Equipment*, 774, 151–158.

[7] Cox, D.R. (1962). *Renewal Theory*. Methuen, London.

[8] Smith., W.L. (1957). On renewal theory, counter problems and quasi-Poisson processes. *Math. Proc. of the Cambridge Philosophical Society*, 53(1), 175–193.

[9] Knoll, G.F. (1999). *Radiation detection and measurement*. John Wiley & Sons.

[10] Arkani, M., Khalafi, H., Arkani, M. (2013). An improved formula for dead time correction of GM detectors. *Nukluinika*, 58(4), 533–536.

[11] Lee, S.H., Gardner, R.P. (2000). A new G-M counter dead time model, Applied Radiation and Isotopes. 53(4–5), 731–737.

[12] Arkani, M. Khalafi, H., Arkani, M., (2013). Efficient dead time correction of G-M counters using feed forward artificial neural network. *Nukluinika*, 58(2), 317−321.

[13] *Modular Pulse-Processing Electronics*. ORTEC Catalog, 2015.

[14] Henzler, S. (2010). *Time-to-Digital Converters*. Springer.

[15] Carbone, P., Kiaei, S., Xu, F. (2014). *Design, Modelling and Testing of Data Converters*.

[16] Zieliński, M., Kowalski, M., *et al.* (2009). Review of single-stage time-interval measurement modules implemented in FPGA devices. *Metrol. Meas. Syst.*, 16(4), 641–648..

[17] Kalisz, J., (2004). Review of Methods for Time Interval Measurements with Picosecond Resolution. *Metrologia*, 41, 17–32.

[18] Kang, L., Zhao, L., *et al*. (2013). A 128-channel high precision time measurement module. *Metrol. Meas. Syst.,* 20(2), 275–286.

[19] Arkani, M., Khalafi, H., Vosoughi, N. (2014). Development of an embedded FPGA-based data acquisition system dedicated to zero power reactor noise experiments. *Metrol. Meas. Syst.,* 21(3), 433–446.

[20] Arkani, M. (2015). *Measurement of Tehran and Esfahan research reactors kinetic parameters using reactor noise diagnostic methods*. Amirkabir University of Technology (Tehran Polytechnique), Nuclear Physics Department, Ph.D. Thesis.

[21] Arkani, M., Khalafi, H., Vosoughi, N., Khakshournia, S. (2015). A FPGA based Time Analyser for Stochastic Methods in Experimental Physics. *Instruments and Experimental Techniques,* 58(3), 350–358.

[22] Grzelak, S., Kowalski, M., *et al*. (2014). High resolution time-interval measurement systems applied to flow measurement. *Metrol. Meas. Syst.*, 21(1), 77–84.

[23] Grzelak, S., Kowalski, M., *et al*. (2014). Ultrasonic flow measurement with high resolution. *Metrol. Meas. Syst.*, 21(2), 305–316.

[24] Zieliński, M., Kowalski, M., *et al*. (2009). Accumulated Jitter Measurement of Standard Clock Oscillators. *Metrol. Meas. Syst.*, 16(2), 259–266.

[25] Artyukh, Y., Boole, E. (2011). Jitter Measurement on the Basis of High-Precision Event Timer. *Metrol. Meas. Syst.*, 18 (3), 453–460.

[26] Zaworski, Ł., Chaberski, D., *et al.* (2012) Quantization error in time-to-digital converters. *Metrol. Meas. Syst.*, 19(1), 115–122.

[27] CYCLONE-III, A Cyclone III Device Handbook, Altera Corporation, 2008.

[28] QUARTUS-II, Handbook Version 9.1, Altera Corporation, 2009.

[29] NIOS II Software Developer's Handbook Version 11.1, (2011). ALTERA Corporation.

[30] Hashimoto, K., Ohya, K., Yamane, Y. (1996). Dead-time measurement for radiation counters by variance-to-mean method. *Journal of Nuclear Science and Technology*, 33(11), 863–868.

[31] Jordan, D.R., McBeth, G.W., (1978). An experimental test of Müller statistics for counting systems with a non-extending dead time. *Nuclear Instruments and Methods*, 155(3), 557–562.

[32] Choi, H.D. (2009). Counting statistics distorted by two dead times in series which end with an extended type dead time. *Nuclear Instruments and Methods in Physics Research Section A: Accelerators, Spectrometers, Detectors and Associated Equipment,* 599(2–3), 251–259.

[33] Arkani, M., Khalafi, H., Vosoughi, N. (2013). A flexible multichannel digital random pulse generator based on FPGA. *World Journal of Nuclear Science and Technology*, 3(4), 109–116.

[34] Landau, D.P. (2000). *A guide to Monte Carlo simulations in statistical physics*. Cambridge University Press.

[35] Dunn, W.L. (2012). *Exploring Monte Carlo methods*. Elsevier, Academic Press.

[36] Mathwroks. (2014). MATLAB reference guide.